論文 / 著書情報
Article / Book Information

Title	Theoretical, numerical and experimental investigation into vibration characteristics for composite structures of an annular membrane internally connected with a piezoceramic disk
Authors	Ming Ji, Jia-Jin Zhong, Yu-Hsi Huang, Yi-Chuang Wu
Citation	Journal of Mechanics, Volume 39, , Page 451–470
Pub. date	2023, 12
DOI	https://doi.org/10.1093/jom/ufad037
Copyright	Information is in the article.

Journal of Mechanics, 2024, **39**, 451–470
https://doi.org/10.1093/jom/ufad037
Advance access publication 4 December 2023
Regular Article

Theoretical, numerical and experimental investigation into vibration characteristics for composite structures of an annular membrane internally connected with a piezoceramic disk

Ming Ji [1], Jia-Jin Zhong [2], Yu-Hsi Huang [3] and Yi-Chuang Wu [2,4,*]

[1]Institute of Innovative Research, Tokyo Institute of Technology, Yokohama, Japan
[2]Department of Mechanical Engineering, National Chung Cheng University, Chiayi, Republic of China
[3]Department of Mechanical Engineering, National Taiwan University, Taipei, Republic of China
[4]Advanced Institute of Manufacturing with High-tech Innovations, National Chung Cheng University, Chiayi, Republic of China

*Corresponding author: imeycwu@ccu.edu.tw

ABSTRACT

This work analyzed the vibration characteristics of an annular membrane internally connected with a piezoceramic disk theoretically, numerically and experimentally. The general solution for the free vibration of an annular membrane under uniform tension was derived. Then, the displacement solutions for the piston modes and coupled modes of an annular membrane internally connected with a piezoceramic disk were derived. Two plate theories, Kirchhoff and Mindlin plate theories, were used to simulate the piezoceramic disk. The theoretical results are compared with the numerical results obtained from two finite element software packages: ABAQUS and COMSOL. The amplitude-fluctuation electronic speckle pattern interferometry was used to measure the resonant frequencies and associated mode shapes of five different type specimens with different sizes. Good agreements of dynamic characteristics determined by theoretical analysis, experimental measurements, and numerical calculation are presented for the annular membrane internally connected with piezoceramic disk structures.

KEYWORDS: analytical solution, annular membrane, piezoceramic disk, AF-ESPI

1. INTRODUCTION

The vibration of an annular membrane internally connected with a piezoceramic disk has gained a lot of interest in recent years. It can be used as a piezoelectric speaker via the inverse piezoelectric effect to produce sound [1]. And it can also be used as high-performance piezo-driven diaphragm micropumps via the piezoelectric effect [2]. Then, Bußmann *et al.* [3] developed a titanium micro diaphragm pump combined with a glued-on piezoelectric disc actuator of microfluidic devices for medical implants. Calderon and Reyes-Betanzo [4] have recently designed a micropump made of a piezoelectric plate and membrane structure to construct a drug delivery system for relieving dry eye disease. Based on the research above, it is evident that efficiently understanding the vibration behavior of membrane and piezoceramic plate composite structures and applying this knowledge to industrial design and dynamic control is an immensely significant issue.

Membranes as structural elements have many applications, such as biological organisms, aerospace craft, etc. The vibration characteristics of the membrane have been investigated by many researchers [5]. The analytical solutions for free vibration of circular and rectangular membranes under uniform tension along the edges were first given by Rayleigh [6]. Mei [7] developed the finite element method to solve the free vibration of circular membranes under arbitrary tension. Nagaya and Hai [8] solved the free vibration of composite membranes with arbitrary shapes. Jabareen and Eisenberger [9] presented solutions for free vibrations of non-homogeneous circular and annular membranes. Bahrami *et al.* [10] applied the wave propagation method to solve the free vibration of annular circular and sectorial membranes. Then, Bahrami and Teimourian [11] used the same way to solve the free vibration of composite, circular annular membranes. Liu *et al.* [12] proposed the dynamic stiffness method to solve the free vibration of membrane assemblies with general classical boundary conditions.

The theoretical analysis of free vibration of piezoelectric plates has been investigated by many researchers [13–18]. To verify the accuracy of those proposed theories, the investigation for piezoceramic materials based on theoretical, numerical, and experimental results is listed in the works [19–23]. Because the performance of energy harvesting systems is highly correlated with the dynamic characteristics of piezoelectric materials, Lien *et al.* [24] utilize the vibration characteristics of four piezoelectric bimorphs to design

Received: 5 November 2023; **Accepted:** 1 December 2023

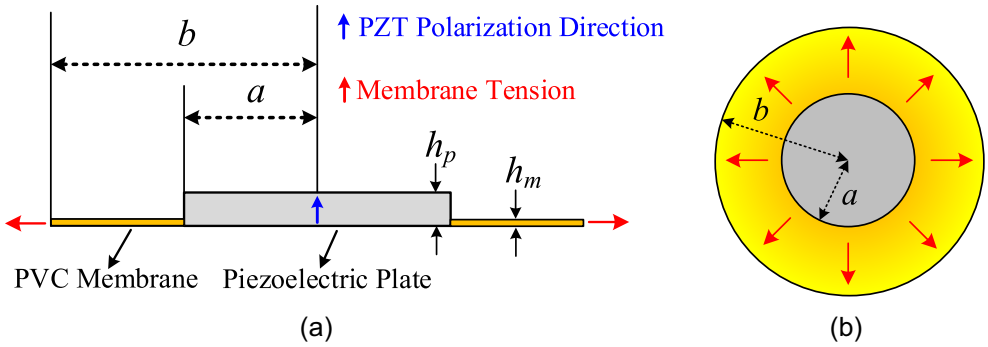

Figure 1 Schematic of an annular membrane internally-connected with a piezoceramic disk (a) side view (b) top view.

two electrical rectifications used for regulating the multiple piezoelectric harvesters. The amplitude-fluctuation electronic speckle pattern interferometry (AF-ESPI) has been widely used to measure the mode shapes of structures. Ma and Huang [25] applied AF-ESPI to get the natural frequencies and in-plane and out-of-plane mode shapes of a piezoelectric block. Then, the same method was used to measure the mode shapes of piezoelectric circular plates [26], annular disks [27], a cross-ply piezo laminated composite plate [28] and two-layered piezoelectric disks [19]. Krushynska *et al.* [29] proposed a theoretical method to control the mode excitation of a rectangular piezoelectric plate, which AF-ESPI verifies.

There are several papers [30–32] investigated the free vibration of annular membranes attached to a central mass. However, they didn't consider the deformation of the main mass. The paper analyzed the vibration characteristics of an annular membrane internally connected with a piezoceramic disk theoretically, numerically and experimentally. The vibration characteristics of the piston motion for the composite structures are also derived and observed from theoretical analysis and experimental measurement. The general solution for the free vibration of an annular membrane under uniform tension was derived first. Then, the solutions for the piston modes and coupled modes of an annular membrane internally connected with a piezoceramic disk were given. Two plate theories, Kirchhoff and Mindlin plate theories, were used to simulate the piezoceramic disk. The theoretical results are compared with the numerical results obtained from two finite element software packages: ABAQUS and COMSOL. Then, the AF-ESPI was used to measure the mode shapes of five specimens with different sizes. The results of the three methods were in good agreement. Furthermore, this analytical solution permits a more complete determination of the plate-membrane composite structure's resonant frequencies and associated mode shapes. This method can be applied to optimize the design of speakers and micropumps efficiently.

2. THEORETICAL ANALYSIS

An annular membrane internally connected with a piezoceramic disk is considered, as Fig. 1 shows. The outer and inner radius of the annular membrane are b and a, and the thickness of the membrane is denoted as h_m. The radius and thickness of the piezoceramic disk are a and h_p, respectively.

For a circular membrane, the equation of motion [33] can be expressed as

$$\frac{\partial^2 w(r,\theta,t)}{\partial r^2}+\frac{1}{r}\frac{\partial w(r,\theta,t)}{\partial r}+\frac{1}{r^2}\frac{\partial^2 w(r,\theta,t)}{\partial \theta^2}=\frac{1}{c_d^2}\frac{\partial^2 w(r,\theta,t)}{\partial t^2}, \tag{1}$$

where w is the transverse displacement; (r,θ) is the polar coordinate system; t is time; $c_d=\sqrt{T/(\rho_m h_m)}$ is the wave speed; ρ_m is the density of the membrane; T is the resultant force per unit length applied on the boundary of the membrane. For the harmonic vibration, the transverse displacement is expressed as

$$w(r,\theta,t)=W(r,\theta)\,e^{i\omega t}, \tag{2}$$

where ω is the angular frequency; $i=\sqrt{-1}$. By substituting Eq. (2) into Eq. (1), the following equation can be obtained.

$$\frac{\partial^2 W(r,\theta)}{\partial r^2}+\frac{1}{r}\frac{\partial W(r,\theta)}{\partial r}+\frac{1}{r^2}\frac{\partial^2 W(r,\theta)}{\partial \theta^2}+k_d^2 W(r,\theta)=0, \tag{3}$$

where $k_d=\omega/c_d$ is the wavenumber. Using the method of separation, the displacement is expressed as

$$W(r,\theta)=R(r)\,\Theta(\theta)\,. \tag{4}$$

By substituting Eq. (4) into Eq. (3), the following equation can be obtained

$$\frac{r^2}{R(r)}\frac{\partial^2 R(r)}{\partial r^2}+\frac{r}{R(r)}\frac{\partial R(r)}{\partial r}+k_d^2 r^2=-\frac{1}{\Theta(\theta)}\frac{\partial^2 \Theta(\theta)}{\partial \theta^2}=n^2, \tag{5}$$

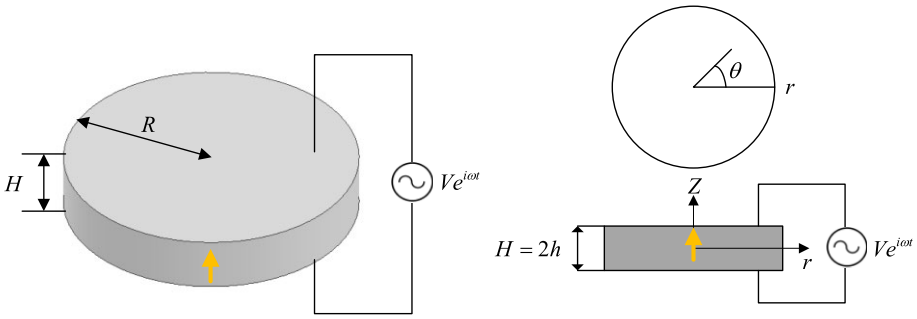

Figure 2 Schematic of a piezoceramic disk.

where n^2 is the constant. Then, Eq. (5) can be rewritten in two dependent equations:

$$\begin{cases} R''(r) + \frac{1}{r}R'(r) + \left(k_d^2 - \frac{n^2}{r^2}\right)R(r) = 0, \\ \Theta''(\theta) + n^2\Theta(\theta) = 0. \end{cases} \tag{6}$$

The general solution can be written as

$$W(r,\theta) = [EJ_n(k_d r) + FY_n(k_d r)]\cos(n\theta), \tag{7}$$

where E and F are unknowns determined by the boundary conditions; J_n and Y_n are Bessel functions of the first and second kind, respectively. For a circular piezoceramic disk with radius R and thickness $H = 2h$ as Fig. 2 shows, the direction of polarization is along the thickness direction.

The e-form constitutive equations of the piezoceramic disk [22] can be expressed as

$$\begin{cases} T_{ij} = C^E_{ijkl}S_{kl} - e_{kij}E_k \\ D_i = e_{ikl}S_{kl} + \varepsilon^S_{ij}E_j \end{cases}, \tag{8}$$

where T_{ij}, S_{kl}, D_i, E_j, C^E_{ijkl}, ε^S_{ij}, and e_{ikl} represent the notation of stress, strain, electric displacement, electric field, stiffness constants, dielectric coefficients and piezoelectric coefficients, respectively. The constitutive equations in the cylindrical coordinate system can be expressed into the matrix form as

$$\begin{bmatrix} T_{rr} \\ T_{\theta\theta} \\ T_{zz} \\ T_{\theta z} \\ T_{rz} \\ T_{r\theta} \\ D_r \\ D_\theta \\ D_z \end{bmatrix} = \begin{bmatrix} c^E_{11} & c^E_{12} & c^E_{13} & 0 & 0 & 0 & 0 & 0 & -e_{31} \\ c^E_{12} & c^E_{11} & c^E_{13} & 0 & 0 & 0 & 0 & 0 & -e_{31} \\ c^E_{13} & c^E_{13} & c^E_{33} & 0 & 0 & 0 & 0 & 0 & -e_{33} \\ 0 & 0 & 0 & c^E_{44} & 0 & 0 & 0 & -e_{15} & 0 \\ 0 & 0 & 0 & 0 & c^E_{44} & 0 & -e_{15} & 0 & 0 \\ 0 & 0 & 0 & 0 & 0 & \frac{1}{2}\left(c^E_{11} - c^E_{12}\right) & 0 & 0 & 0 \\ 0 & 0 & 0 & 0 & e_{15} & 0 & \varepsilon^S_{11} & 0 & 0 \\ 0 & 0 & 0 & e_{15} & 0 & 0 & 0 & \varepsilon^S_{11} & 0 \\ e_{31} & e_{31} & e_{33} & 0 & 0 & 0 & 0 & 0 & \varepsilon^S_{33} \end{bmatrix} \begin{bmatrix} S_{rr} \\ S_{\theta\theta} \\ S_{zz} \\ 2S_{\theta z} \\ 2S_{rz} \\ 2S_{r\theta} \\ E_r \\ E_\theta \\ E_z \end{bmatrix}, \tag{9}$$

where C^E_{pq} and e_{iq} are Voigt notations of C^E_{ijkl} and e_{ikl}, respectively. The equations of motion in cylindrical coordinate system can be expressed as

$$\frac{\partial T_{rr}}{\partial r} + \frac{1}{r}\frac{\partial T_{r\theta}}{\partial \theta} + \frac{1}{r}(T_{rr} - T_{\theta\theta}) + \frac{\partial T_{rz}}{\partial z} - \rho\frac{\partial^2 u_r}{\partial t^2} = 0, \tag{10}$$

$$\frac{\partial T_{r\theta}}{\partial r} + \frac{1}{r}\frac{\partial T_{\theta\theta}}{\partial \theta} + \frac{2}{r}T_{r\theta} + \frac{\partial T_{\theta z}}{\partial z} - \rho\frac{\partial^2 u_\theta}{\partial t^2} = 0, \tag{11}$$

$$\frac{\partial T_{rz}}{\partial r} + \frac{1}{r}\frac{\partial T_{\theta z}}{\partial \theta} + \frac{1}{r}T_{rz} + \frac{\partial T_{zz}}{\partial z} - \rho\frac{\partial^2 u_z}{\partial t^2} = 0. \tag{12}$$

The strain-displacement relationship is

$$S_{rr} = \frac{\partial u_r}{\partial r}, \quad S_{\theta\theta} = \frac{u_r}{r} + \frac{1}{r}\frac{\partial u_\theta}{\partial \theta}, \quad S_{zz} = \frac{\partial u_z}{\partial z},$$
$$2S_{r\theta} = \frac{1}{r}\frac{\partial u_r}{\partial \theta} + \frac{\partial u_\theta}{\partial r} - \frac{u_\theta}{r}, \quad 2S_{rz} = \frac{\partial u_r}{\partial z} + \frac{\partial u_z}{\partial r}, \quad 2S_{\theta z} = \frac{\partial u_\theta}{\partial z} + \frac{1}{r}\frac{\partial u_z}{\partial \theta}. \tag{13}$$

The relationship between electric fields and electric potential is

$$E_r = -\frac{\partial \varphi}{\partial r}, \quad E_\theta = -\frac{1}{r}\frac{\partial \varphi}{\partial \theta}, \quad E_z = -\frac{\partial \varphi}{\partial z}, \tag{14}$$

where φ is the electric potential. The electrostatic equation is

$$\frac{\partial D_r}{\partial r} + \frac{D_r}{r} + \frac{1}{r}\frac{\partial D_\theta}{\partial \theta} + \frac{\partial D_z}{\partial z} = 0. \tag{15}$$

The normal stress in the thickness direction is ignored, $T_{zz} = 0$, which gives

$$S_{zz} = -\frac{c_{13}^E}{c_{33}^E}(S_{rr} + S_{\theta\theta}) + \frac{e_{33}}{c_{33}^E}E_z. \tag{16}$$

By substituting Eq. (16) into Eq. (9), the constitutive equation can be rewritten in

$$\begin{bmatrix} T_{rr} \\ T_{\theta\theta} \\ T_{\theta z} \\ T_{rz} \\ T_{r\theta} \\ D_r \\ D_\theta \\ D_z \end{bmatrix} = \begin{bmatrix} \tilde{c}_{11}^E & \tilde{c}_{12}^E & 0 & 0 & 0 & 0 & 0 & -\tilde{e}_{31} \\ \tilde{c}_{12}^E & \tilde{c}_{11}^E & 0 & 0 & 0 & 0 & 0 & -\tilde{e}_{31} \\ 0 & 0 & c_{55}^E & 0 & 0 & 0 & -e_{15} & 0 \\ 0 & 0 & 0 & c_{55}^E & 0 & -e_{15} & 0 & 0 \\ 0 & 0 & 0 & 0 & \frac{1}{2}(\tilde{c}_{11}^E - \tilde{c}_{12}^E) & 0 & 0 & 0 \\ 0 & 0 & 0 & e_{15} & 0 & \varepsilon_{11}^S & 0 & 0 \\ 0 & 0 & e_{15} & 0 & 0 & 0 & \tilde{\varepsilon}_{33}^S & 0 \\ \tilde{e}_{31} & \tilde{e}_{31} & 0 & 0 & 0 & 0 & 0 & \tilde{\varepsilon}_{33}^S \end{bmatrix} \begin{bmatrix} S_{rr} \\ S_{\theta\theta} \\ 2S_{\theta z} \\ 2S_{rz} \\ 2S_{r\theta} \\ E_r \\ E_\theta \\ E_z \end{bmatrix}, \tag{17}$$

where

$$\tilde{c}_{11}^E = c_{11}^E - \left(c_{13}^E\right)^2 / c_{33}^E, \quad \tilde{c}_{12}^E = c_{12}^E - \left(c_{13}^E\right)^2 / c_{33}^E,$$
$$\tilde{e}_{31} = e_{31} - e_{33}c_{13}^E / c_{33}^E, \quad \tilde{\varepsilon}_{33}^S = \varepsilon_{33}^S + (e_{33})^2 / c_{33}^E. \tag{18}$$

The piezoceramic disk's free vibration problems can be solved using the Mindlin plate theory and Kirchhoff plate theory [21]. There are two types of vibration behaviors for the free vibration of an annular membrane internally connected with a piezoceramic disk; one is called "piston mode," and the other is known as "coupled mode." As the structure acts in the piston motion, the piezoceramic disk is undeformed and considered a mass load. In other words, the vibration behavior of the piston mode is dominated by the part of the annular membrane. When the structure vibrates in a coupled mode, the dynamic behavior of the membrane and the disk mutually influence each other. Therefore, it is necessary to consider the continuity of the displacement field between the annular membrane and the piezoceramic disk.

2.1. Piston mode

For the "piston mode," the displacement of the disk's rigid motion is $W_1(t)$, and the displacement of the membrane is $W_2(r, \theta)$ as Eq. (7) shows. The outer boundary condition of the annular membrane is fixed, then the displacement function of $W_2(r, \theta)$ along the edge $r = b$ can be given as

$$W_2(r, \theta)\big|_{r=b} = 0. \tag{19}$$

By substituting Eq. (7) into Eq. (19), the solution can be rewritten as

$$W_2(r, \theta) = -\frac{F}{J_n(k_d b)}\left[Y_n(k_d b)\, J_n(k_d r) - J_n(k_d b)\, Y_n(k_d r)\right]\cos(n\theta). \tag{20}$$

The force applied on the inner boundary of the membrane F_{inner}^{mem} is the inertial force of the disk. Then, the equations of motion of the piston mode can be given as

$$F_{inner}^{mem} = 2\pi a T \left.\frac{\partial w_2(r, \theta, t)}{\partial r}\right|_{r=a} = M_p \left.\frac{\mathrm{d}^2 w_1(r, \theta, t)}{\mathrm{d}t^2}\right|_{r=a}, \tag{21}$$

where $M_p = a^2\pi h_p \rho_p$ is the mass of the disk; h_p is the thickness of the disk; ρ_p is the density of the disk; $w_1(r,\theta,t)$ is the displacement of the disk; and $w_2(r,\theta,t)$ is the displacement of the membrane. The continuity condition of the displacement is

$$w_1(r,\ \theta,\ t)\big|_{r=a} = w_2(r,\ \theta,t)\big|_{r=a}. \tag{22}$$

By substituting Eq. (22) and the harmonic vibration. $w_2(r,\theta,t) = W_2(r,\theta)e^{i\omega t}$. into Eq. (21), the following equation is obtained

$$2\pi aT\left.\frac{\partial W_2(r,\theta)}{\partial r}\right|_{r=a} = -\omega^2 M_p W_2(a,\theta)\,. \tag{23}$$

The characteristic function can be obtained by substituting Eq. (20) into Eq. (23):

$$\begin{aligned} &2\pi aTk_d\left\{Y_n(k_d b)\left[-J_{n+1}(k_d a)+\frac{n}{k_d a}J_n(k_d a)\right]-J_n(k_d b)\left[-Y_{n+1}(k_d a)+\frac{n}{k_d a}Y_n(k_d a)\right]\right\}\\ &= -\omega^2 M_p\left[Y_n(k_d b)\,J_n(k_d a)-J_n(k_d b)\,Y_n(k_d a)\right]. \end{aligned} \tag{24}$$

To solve the eigenvalue equation of Eq. (24), the resonant frequencies and mode shapes of piston modes can be obtained.

2.2. Coupled mode

2.2.1. Mindlin plate theory

The solution of the free vibration for the piezoceramic disk based on Mindlin plate theory is

$$W_1 = \sum_{j=1}^{2} C_j \bar{W}_j^1\left(\alpha_j\xi\right), \tag{25}$$

where C_j are the undetermined constants; the details of coefficients α_j can be found in [21]; $\xi = r/a$. For the Mindlin plate theory, there are three undetermined constants. The third undetermined constant is associated with the slope rotations. The detail of solution can also been found in [21]. The method of solving the problem can also be found in [34], [35]. The outer boundary condition of the annular membrane is the same with Eq. (19). The continuity condition of the displacement is

$$W_1(r,\theta)\big|_{r=a} = W_2(r,\theta)\big|_{r=a}. \tag{26}$$

Since the membrane element is soft and can not sustain the bending moment, the boundary conditions of force terms between piezoceramic disk and annular membrane at $r = a$ can be given as

$$M_{rr}(r)\big|_{r=a} = M_{r\theta}(r)\big|_{r=a} = Q_r(r)\big|_{r=a} = 0, \tag{27}$$

where M_{rr} is the bending moment; $M_{r\theta}$ is the shear moment; and Q_r is the shear force. Substituting the solutions in Eqs. (7) and (25) into the boundary conditions and continuity conditions, the following equations are obtained:

$$EJ_n(k_d b) + FY_n(k_d b) = 0, \tag{28}$$

$$EJ_n(k_d a) + FY_n(k_d a) = aC_1\bar{W}_1(\alpha_1) + aC_2\bar{W}_2(\alpha_2)\,, \tag{29}$$

$$\begin{aligned} &\left\{\sum_{j=2}^{2}\frac{\bar{\chi}_j}{a}\left[D_1\frac{\partial^2\bar{W}_j(\alpha_j\xi)}{\partial\xi^2}+(D_1-2A_1)\left(\frac{\partial\bar{W}_j(\alpha_j\xi)}{\xi\,\partial\xi}-\frac{n^2}{\xi^2}\bar{W}_j(\alpha_j\xi)\right)+A_5x_j\bar{W}_j(\alpha_j\xi)\right]C_j\right.\\ &\left.-2\frac{A_1}{a}\left(\frac{n}{\xi^2}\bar{W}_3(\alpha_3\xi)-\frac{n}{\xi}\frac{\partial\bar{W}_3(\alpha_3\xi)}{\partial\xi}\right)C_3\right\}\Bigg|_{\xi=1} = 0, \end{aligned} \tag{30}$$

$$\left\{\sum_{j=1}^{2}\frac{2A_1\bar{\chi}_j}{a}\left(\frac{n}{\xi^2}\bar{W}_j(\alpha_j\xi)-\frac{n}{\xi}\frac{\partial\bar{W}_j}{\partial\xi}(\alpha_j\xi)\right)C_i+\frac{A_1}{a}\left(-\frac{\partial^2\bar{W}_3}{\partial\xi^2}(\alpha_3\xi)+\frac{\partial\bar{W}_3}{\xi\,\partial\xi}(\alpha_3\xi)-\frac{n^2}{\xi^2}\bar{W}_3(\alpha_3\xi)\right)C_3\right\}\Bigg|_{\xi=1} = 0, \tag{31}$$

$$\left\{\sum_{j=1}^{2}\left[A_3\left(\bar{\chi}_j+1\right)\frac{\partial\bar{W}_j}{\partial\xi}(\alpha_j\xi)\right]C_j+\left[A_3\frac{n}{\xi}\bar{W}_3(\alpha_3\xi)\right]C_3\right\}\Bigg|_{\xi=1} = 0. \tag{32}$$

The Eqs. (28)–(32) can be rewritten in matrix form

$$\begin{bmatrix} A_{11} & A_{12} & A_{13} & A_{14} & A_{15} \\ A_{21} & A_{22} & A_{23} & A_{24} & A_{25} \\ A_{31} & A_{32} & A_{33} & A_{34} & A_{35} \\ A_{41} & A_{42} & A_{43} & A_{44} & A_{45} \\ A_{51} & A_{52} & A_{53} & A_{54} & A_{55} \end{bmatrix} \begin{bmatrix} E \\ F \\ C_1 \\ C_2 \\ C_3 \end{bmatrix} = \begin{bmatrix} 0 \\ 0 \\ 0 \\ 0 \\ 0 \end{bmatrix}, \tag{33}$$

where

$$A_{11} = J_n(k_d b), \quad A_{12} = Y_n(k_d b), \quad A_{13} = A_{14} = A_{15} = 0, \tag{34}$$

$$A_{21} = J_n(k_d a), \quad A_{22} = Y_n(k_d a), \quad A_{23} = -b\bar{W}_1(\alpha_1), \quad A_{24} = -b\bar{W}_2(\alpha_2), \quad A_{25} = 0, \tag{35}$$

$$\begin{aligned} A_{31} &= A_{32} = 0, \\ A_{33} &= \bar{\chi}_1 \left[\frac{D_1}{a} \frac{\partial^2 \bar{W}_1(\alpha_1 \xi)}{\partial \xi^2} + \frac{(D_1 - 2A_1)}{a} \left(\frac{\partial \bar{W}_1(\alpha_1 \xi)}{\partial \xi} - n^2 \bar{W}_1(\alpha_1 \xi) \right) + \frac{A_5}{a} x_1 \bar{W}_1(\alpha_1 \xi) \right] \Big|_{\xi=1}, \\ A_{34} &= \bar{\chi}_2 \left[\frac{D_1}{a} \frac{\partial^2 \bar{W}_2(\alpha_2 \xi)}{\partial \xi^2} + \frac{(D_1 - 2A_1)}{a} \left(\frac{\partial \bar{W}_2(\alpha_2 \xi)}{\partial \xi} - n^2 \bar{W}_2(\alpha_2 \xi) \right) + \frac{A_5}{a} x_2 \bar{W}_2(\alpha_2 \xi) \right] \Big|_{\xi=1}, \\ A_{35} &= \frac{-2A_1}{a} \left(\frac{n}{\xi^2} \bar{W}_3(\alpha_3 \xi) - \frac{n}{\xi} \frac{\partial \bar{W}_3(\alpha_3 \xi)}{\partial \xi} \right) \Big|_{\xi=1}, \end{aligned} \tag{36}$$

$$\begin{aligned} A_{41} &= A_{42} = 0, \\ A_{43} &= \frac{2A_1 \bar{\chi}_1}{a} \left(\frac{n}{\xi^2} \bar{W}_1(\alpha_1 \xi) - \frac{n}{\xi} \frac{\partial \bar{W}_1}{\partial \xi}(\alpha_1 \xi) \right) \Big|_{\xi=1}, \\ A_{44} &= \frac{2A_1 \bar{\chi}_2}{a} \left(\frac{n}{\xi^2} \bar{W}_2(\alpha_2 \xi) - \frac{n}{\xi} \frac{\partial \bar{W}_2}{\partial \xi}(\alpha_2 \xi) \right) \Big|_{\xi=1}, \\ A_{45} &= \frac{A_1}{a} \left[-\frac{\partial^2 \bar{W}_3(\alpha_3 \xi)}{\partial \xi^3} + \frac{\partial \bar{W}_3(\alpha_3 \xi)}{\partial \xi} - n^2 \bar{W}_3(\alpha_3 \xi) \right] \Big|_{\xi=1}, \end{aligned} \tag{37}$$

$$A_{51} = A_{52} = 0, \quad A_{53} = \left[A_3(\bar{\chi}_1 + 1) \frac{\partial \bar{W}_1}{\partial \xi}(\alpha_1 \xi) \right] \Big|_{\xi=1}, \quad A_{54} = \left[A_3(\bar{\chi}_2 + 1) \frac{\partial \bar{W}_2}{\partial \xi}(\alpha_2 \xi) \right] \Big|_{\xi=1}, \quad A_{55} = A_3 n \bar{W}_3(\alpha_3). \tag{38}$$

The details of coefficients $A_1, A_3, A_5, D_1, \bar{\chi}_1, \bar{\chi}_2, \alpha_3, x_1$ and x_2 can be found in [21]. As the annular frequency equals to the resonant frequencies, the determinant of matrix in Eq. (33) equals to 0.

2.2.2. *Kirchhoff plate theory*

The solution of the free vibration for the piezoceramic disk based on Kirchhoff plate theory is

$$W_1 = C_1 J_n(\alpha_1 \xi) + C_2 I_n(\alpha_2 \xi), \tag{39}$$

where $\alpha_{1,2} = \sqrt{|x_{1,2}|}$; $x_1 = -\sqrt{(2\rho h \omega^2 R^4)/(D_1 + A_5)}$; $x_2 = \sqrt{(2\rho h \omega^2 R^4)/(D_1 + A_5)}$. The boundary conditions of the piezoceramic disk at $r = a$ are given as

$$M_{rr}(r)\big|_{r=a} = V_r(r)\big|_{r=a} = 0. \tag{40}$$

Substituting the solutions in Eqs. (7) and (39) into the boundary conditions and continuity condition, the following equations are obtained:

$$E J_n(k_d b) + F Y_n(k_d b) = 0, \tag{41}$$

$$E J_n(k_d a) + F Y_n(k_d a) = a J_n(\alpha_1) + a I_n(\alpha_1), \tag{42}$$

$$-\frac{2h^3}{3a} \left[\bar{c}_{11}^E \frac{\partial^2 W_1}{\partial \xi^2} + \bar{c}_{12}^E \left(\frac{\partial W_1}{\xi \partial \xi} - \frac{n^2}{\xi^2} W_1 \right) + \frac{\bar{e}_{31}^2}{\bar{\varepsilon}_{33}^S} \widehat{\Delta} W_1 \right] \Big|_{\xi=1} = 0, \tag{43}$$

$$\left[-\frac{2h^3}{3a^2} \left(\bar{c}_{11}^E + \frac{\bar{e}_{31}^2}{\bar{\varepsilon}_{33}^S} \right) \frac{\partial}{\partial \xi} \widehat{\Delta} W_1 - \frac{2h^3}{3a^2} n^2 \left(\bar{c}_{11}^E - \bar{c}_{12}^E \right) \left(\frac{W_1}{\xi^3} - \frac{\partial W_1}{\xi^2 \partial \xi} \right) \right] \Big|_{\xi=1} = 0. \tag{44}$$

Table 1 Material properties of PVC membrane.

Property		Value
Density(kg/m^3)	ρ_m	1230
Elastic modulus (GPa)	E	0.841
Poisson's ratio	ν	0.3

Table 2 Material properties of PIC-255.

Property		Values
Density(kg/m^3)	ρ	7750
Dielectric constants (F/m)	ε_{11}^S	8.287×10^{-9}
	ε_{33}^S	6.72×10^{-9}
Elastic constants (N/m^2)	c_{11}^E	1.225×10^{11}
	c_{12}^E	7.867×10^{11}
	c_{13}^E	8.563×10^{10}
	c_{33}^E	1.192×10^{11}
	c_{66}^E	2.1915×10^{10}
	c_{44}^E	2.128×10^{10}
Piezoelectric stress constants (C/m^2)	e_{15}	13.14
	e_{31}	−6.73
	e_{33}	15.68

Table 3 Geometric sizes of different specimen.

Theory	Type A	Type B	Type C	Type D	Type E
a (mm)	28	25	28	12.5	10
R (mm)	28	25	28	12.5	10
b (mm)	53	53	38	25	25
FEM	**Type A**	**Type B**	**Type C**	**Type D**	**Type E**
a (mm)	28	25	28	12.5	10
R (mm)	25	22	25	9.5	7
b (mm)	53	53	38	25	25

The matrix form of Eqs. (41)–(44) is

$$\begin{bmatrix} A_{11} & A_{12} & A_{13} & A_{14} \\ A_{21} & A_{22} & A_{23} & A_{24} \\ A_{31} & A_{32} & A_{33} & A_{34} \\ A_{41} & A_{42} & A_{43} & A_{44} \end{bmatrix} \begin{bmatrix} E \\ F \\ C_1 \\ C_2 \end{bmatrix} = \begin{bmatrix} 0 \\ 0 \\ 0 \\ 0 \end{bmatrix}, \tag{45}$$

where the elements in Eq. (45) can be listed as below:

$$A_{11} = J_n(k_d b), \quad A_{12} = Y_n(k_d b), \quad A_{13} = A_{14} = 0, \tag{46}$$

$$A_{21} = J_n(k_d a), \quad A_{22} = Y_n(k_d a), \quad A_{23} = -aJ_n(\alpha), \quad A_{24} = -aI_n(\alpha), \tag{47}$$

$$\begin{aligned} &A_{31} = A_{32} = 0, \\ &A_{33} = -\frac{2h^3}{3a}\left(\bar{c}_{11}^E + \frac{\bar{e}_{31}^2}{\bar{\varepsilon}_{33}^S}\right) x_1 J_n(\alpha) + \frac{2h^3}{3a}\left(\bar{c}_{11}^E - \bar{c}_{12}^E\right)\left[\frac{\alpha}{2}\left(J_{n-1}(\alpha) - J_{n+1}(\alpha)\right) - n^2 J_n(\alpha)\right], \\ &A_{34} = -\frac{2h^3}{3a}\left(\bar{c}_{11}^E + \frac{\bar{e}_{31}^2}{\bar{\varepsilon}_{33}^S}\right) x_2 I_n(\alpha) + \frac{2h^3}{3a}\left(\bar{c}_{11}^E - \bar{c}_{12}^E\right)\left[\frac{\alpha}{2}\left(I_{n-1}(\alpha) + I_{n+1}(\alpha)\right) - n^2 I_n(\alpha)\right]; \end{aligned} \tag{48}$$

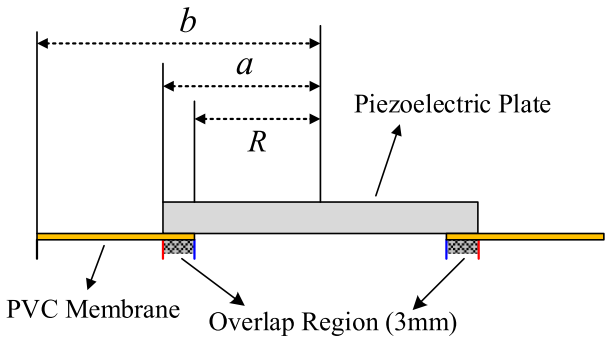

Figure 3 Schematic of a geometric model used in FEM.

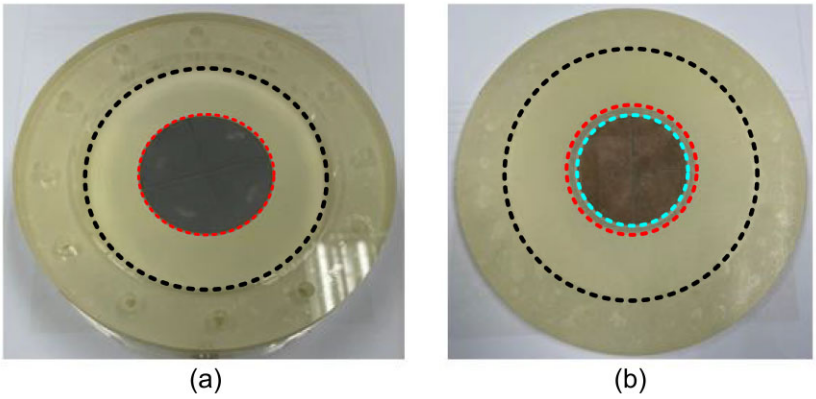

Figure 4 The composite structure of membrance and PZT plate (a) top view (b) bottom view.

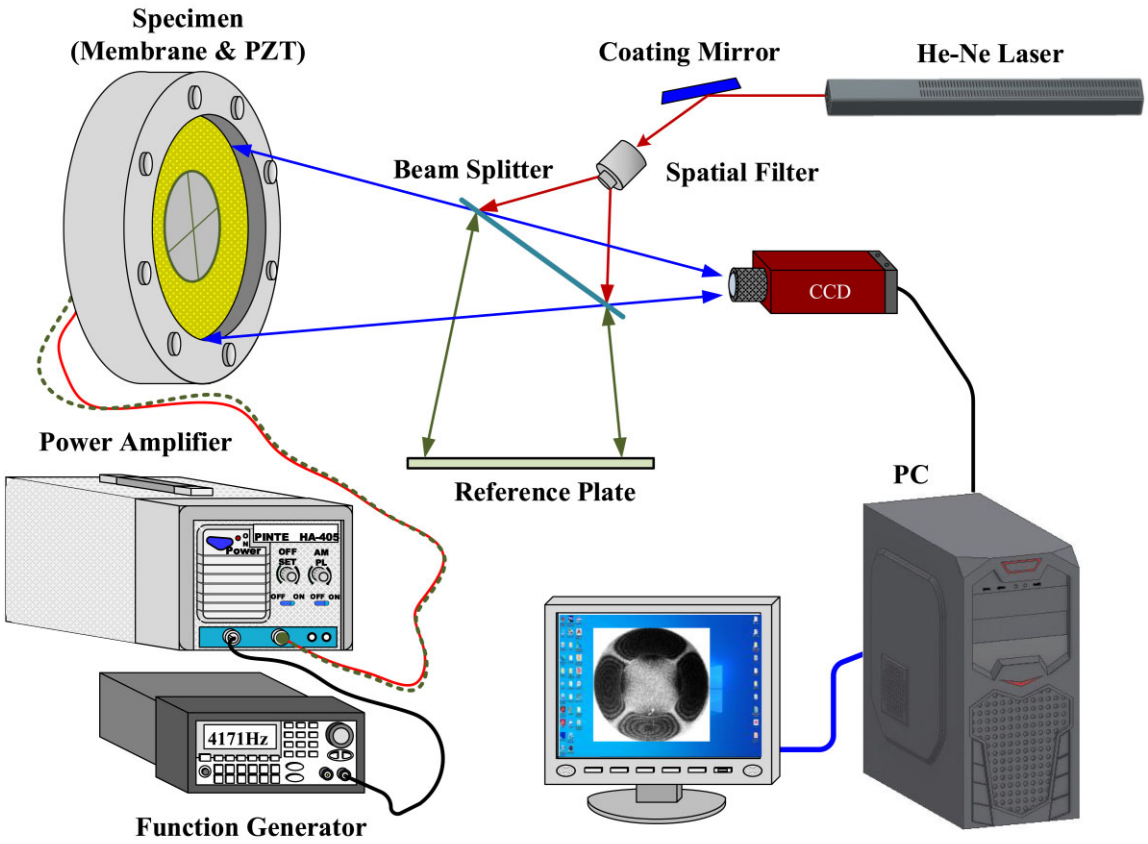

Figure 5 Schematic of the AF-ESPI measurement technique for measuring flexural mode shapes.

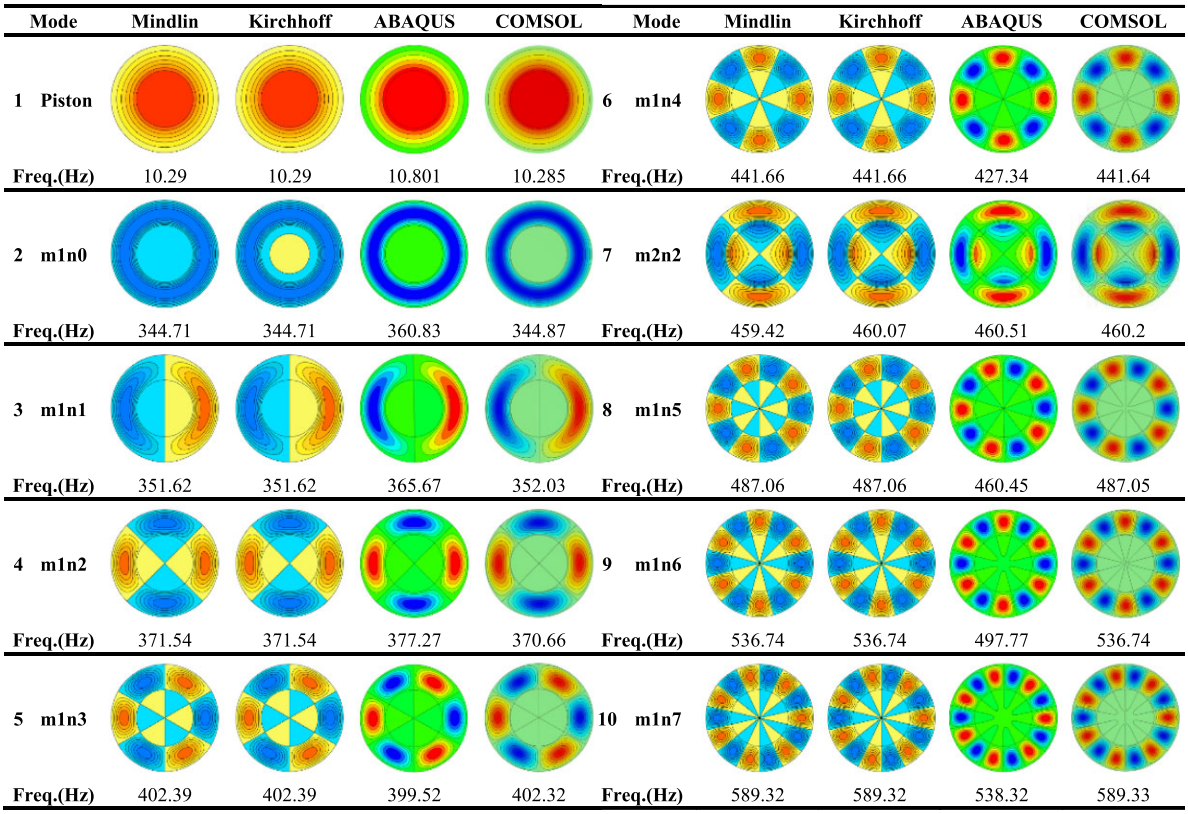

Figure 6 The first ten modes comparison result of type A structure obtained from theory and FEM.

Table 4 First 10 resonant frequencies of type A.

	Frequency (Hz)				
Mode	**Mindlin**	**ABAQUS**	**Diff (%)**	**COMSOL**	**Diff (%)**
1	10.29	10.801	−4.97	10.285	0.05
2	344.71	360.83	−4.68	344.87	−0.05
3	351.62	365.67	−4.00	352.03	−0.12
4	371.54	377.27	−1.54	370.66	0.24
5	402.39	399.52	0.71	402.32	0.02
6	441.66	427.34	3.24	441.64	0.005
7	459.42	460.51	−0.23	460.2	−0.17
8	487.06	460.45	5.46	487.05	0.002
9	536.74	497.77	7.26	536.74	0
10	589.32	538.32	8.65	589.33	−0.002
	Frequency (Hz)				
Mode	**Kirchhoff**	**ABAQUS**	**Diff (%)**	**COMSOL**	**Diff (%)**
1	10.29	10.801	−4.97	10.285	0.05
2	344.71	360.83	−4.68	344.87	−0.05
3	351.62	365.67	−4.00	352.03	−0.12
4	371.54	377.27	−1.54	370.66	0.24
5	402.39	399.52	0.71	402.32	0.02
6	441.66	427.34	3.24	441.64	0.005
7	460.07	460.51	−0.1	460.2	−0.03
8	487.06	460.45	5.46	487.05	0.002
9	536.74	497.77	7.26	536.74	0
10	589.32	538.32	8.65	589.33	−0.002

Table 5 First 10 natural frequencies of free piezoceramic disk and clamped-clamped annular membrane.

	Piezoceramic disk		Annular membrane	
Mode	**ABAQUS (Hz)**	**COMSOL (Hz)**	**ABAQUS (Hz)**	**COMSOL (Hz)**
1	459.18	459.22	363.95	344.71
2	989.66	989.91	368.02	351.63
3	1085	1085.4	379.95	371.54
4	1927.7	1928.7	399.01	402.39
5	2160.2	2161.3	424.22	441.66
6	2982.6	2985.1	454.5	487.06
7	3644	3647.3	488.87	536.74
8	4047.4	4048.6	526.46	589.33
9	4245.7	4250.5	566.57	643.81
10	5415.3	5422.9	729.19	692

Table 6 First 10 resonant frequencies of type B.

	Frequency (Hz)				
Mode	**Mindlin**	**ABAQUS**	**Diff (%)**	**COMSOL**	**Diff (%)**
1	11.87	12.466	−5.02	11.859	0.09
2	307.2	321.71	−4.72	307.44	−0.08
3	315.65	328	−3.91	316.2	−0.17
4	339.63	343.45	−1.12	338.93	0.21
5	375.84	370.91	1.31	375.78	0.02
6	420.7	405.08	3.71	420.68	0.005
7	461.11	460.51	0.13	461.54	−0.09
8	471.21	444.8	5.6	471.2	0.002
9	525.21	488.55	6.98	525.2	0.002
10	581.23	535.13	7.93	581.23	0
	Frequency (Hz)				
Mode	**Kirchhoff**	**ABAQUS**	**Diff (%)**	**COMSOL**	**Diff (%)**
1	11.87	12.466	−5.02	11.859	0.09
2	307.2	321.71	−4.72	307.44	−0.08
3	315.65	328	−3.91	316.2	−0.17
4	339.63	343.45	−1.12	338.93	0.21
5	375.84	370.91	1.31	375.78	0.02
6	420.7	405.08	3.71	420.68	0.005
7	461.69	460.51	0.26	461.54	0.03
8	471.21	444.8	5.6	471.2	0.002
9	525.21	488.55	6.98	525.2	0.002
10	581.23	535.13	7.93	581.23	0

$$
\begin{aligned}
&A_{41} = A_{42} = 0,\\
&A_{43} = -\frac{2h^3}{3a^2}\left(\tilde{c}_{11}^E + \frac{\tilde{e}_{31}^2}{\tilde{\varepsilon}_{33}^S}\right)\varkappa_1\frac{\alpha}{2}\left[J_{n-1}(\alpha) - J_{n+1}(\alpha)\right] - \frac{2h^3}{3a^2}\left(\tilde{c}_{11}^E - \tilde{c}_{12}^E\right)n^2\left[J_n(\alpha) - \frac{\alpha}{2}\left(J_{n-1}(\alpha) - J_{n+1}(\alpha)\right)\right],\\
&A_{44} = -\frac{2h^3}{3a^2}\left(\tilde{c}_{11}^E + \frac{\tilde{e}_{31}^2}{\tilde{\varepsilon}_{33}^S}\right)\varkappa_1\frac{\alpha}{2}\left[I_{n-1}(\alpha) + I_{n+1}(\alpha)\right] - \frac{2h^3}{3a^2}\left(\tilde{c}_{11}^E - \tilde{c}_{12}^E\right)n^2\left[I_n(\alpha) - \frac{\alpha}{2}\left(I_{n-1}(\alpha) + I_{n+1}(\alpha)\right)\right].
\end{aligned}
\tag{49}
$$

Similarly, the resonant frequencies will cause the determinant of the matrix in Eq. (45) to be equal to 0. After the resonant frequencies have been found, the ratio of those undetermined coefficients in Eqs. (33) and (45) can also be obtained. Finally, the associated mode shapes based on Mindlin and Kirchhoff plate theories can be given by substituting the coefficients into Eqs. (7) and (25), and into Eqs. (7) and (39), respectively.

3. RESULTS AND DISCUSSION

3.1. Experimental setup and numerical simulation

In the experiments, polyvinyl chloride (PVC) membrane is used. The material properties of PVC membrane are shown in Table 1. The thickness of the membrane is 0.011 mm. The surface tension T is equal to 4.06 N/m. The material of the piezoceramic disk is PIC-255. The material properties of PIC-255 are shown in Table 2. The double-sided tape is used to connect the PVC membrane

Table 7 First 10 resonant frequencies of type C.

	Frequency (Hz)				
Mode	**Mindlin**	**ABAQUS**	**Diff (%)**	**COMSOL**	**Diff (%)**
1	14.88	15.376	−3.33	14.874	0.04
2	459.42	459.69	−0.06	459.75	−0.07
3	865.11	890.67	−2.95	863.82	0.15
4	869.18	895.1	−2.98	869.52	−0.03
5	881.25	902	−2.35	882	−0.09
6	901	909.95	−0.99	899.52	0.16
7	927.93	926.15	0.19	927.71	0.02
8	961.43	944.79	1.73	961.35	0.01
9	989.77	991.86	−0.21	991.33	−0.016
10	1000.82	966.94	3.39	1000.8	0.002
	Frequency (Hz)				
Mode	**Kirchhoff**	**ABAQUS**	**Diff (%)**	**COMSOL**	**Diff (%)**
1	14.88	15.376	−3.33	14.874	0.04
2	460.07	459.69	0.08	459.75	0.07
3	865.11	890.67	−2.95	863.82	0.15
4	869.18	895.1	−2.98	869.52	−0.03
5	881.25	902	−2.35	882	−0.09
6	901	909.95	−0.99	899.52	0.16
7	927.93	926.15	0.19	927.71	0.02
8	961.43	944.79	1.73	961.35	0.01
9	990.22	991.86	−0.17	991.33	−0.11
10	1000.82	966.94	3.39	1000.8	0.002

Table 8 First 10 resonant frequencies of type D.

	Frequency (Hz)				
Mode	**Mindlin**	**ABAQUS**	**Diff (%)**	**COMSOL**	**Diff (%)**
1	34.9	36.181	−3.67	34.824	0.22
2	688.81	714.02	−3.66	689.68	−0.13
3	705.03	727.75	−3.22	707.24	−0.31
4	751.43	754.45	−0.4	746.67	0.63
5	822.43	815.21	0.88	822.07	0.04
6	911.65	886.54	2.75	911.55	0.01
7	922.23	928.19	−0.65	927.11	−0.52
8	1013.47	969.56	4.33	1013.4	0.007
9	1123.63	1061.2	5.56	1123.6	0.003
10	1239.07	1158.9	6.47	1239.1	−0.002
	Frequency (Hz)				
Mode	**Kirchhoff**	**ABAQUS**	**Diff (%)**	**COMSOL**	**Diff (%)**
1	34.9	36.181	−3.67	34.824	0.22
2	688.81	714.02	−3.66	689.68	−0.13
3	705.03	727.75	−3.22	707.24	−0.31
4	751.43	754.45	−0.4	746.67	0.63
5	822.43	815.21	0.88	822.07	0.04
6	911.65	886.54	2.75	911.55	0.01
7	923.38	928.19	−0.52	927.11	−0.4
8	1013.47	969.56	4.33	1013.4	0.007
9	1123.63	1061.2	5.56	1123.6	0.003
10	1239.07	1158.9	6.47	1239.1	−0.002

and piezoceramic disk. The overlapping part is 3 mm. In the numerical simulations, two commercial finite element software are used: ABAQUS and COMSOL. The geometric model used in the finite element method (FEM) is shown in Fig. 3. Five specimens are used in the experiments and numerical simulations. The geometric sizes of different specimen are shown in Table 3. The thicknesses of the piezoceramic disks in types A and C are 0.5 mm. And the thicknesses of the piezoceramic disks in types B, D and E are 0.4, 0.2, and 0.2 mm, respectively. An experimental specimen is shown in Fig. 4. The region between the black and red dotted lines, given in Fig. 4(a),

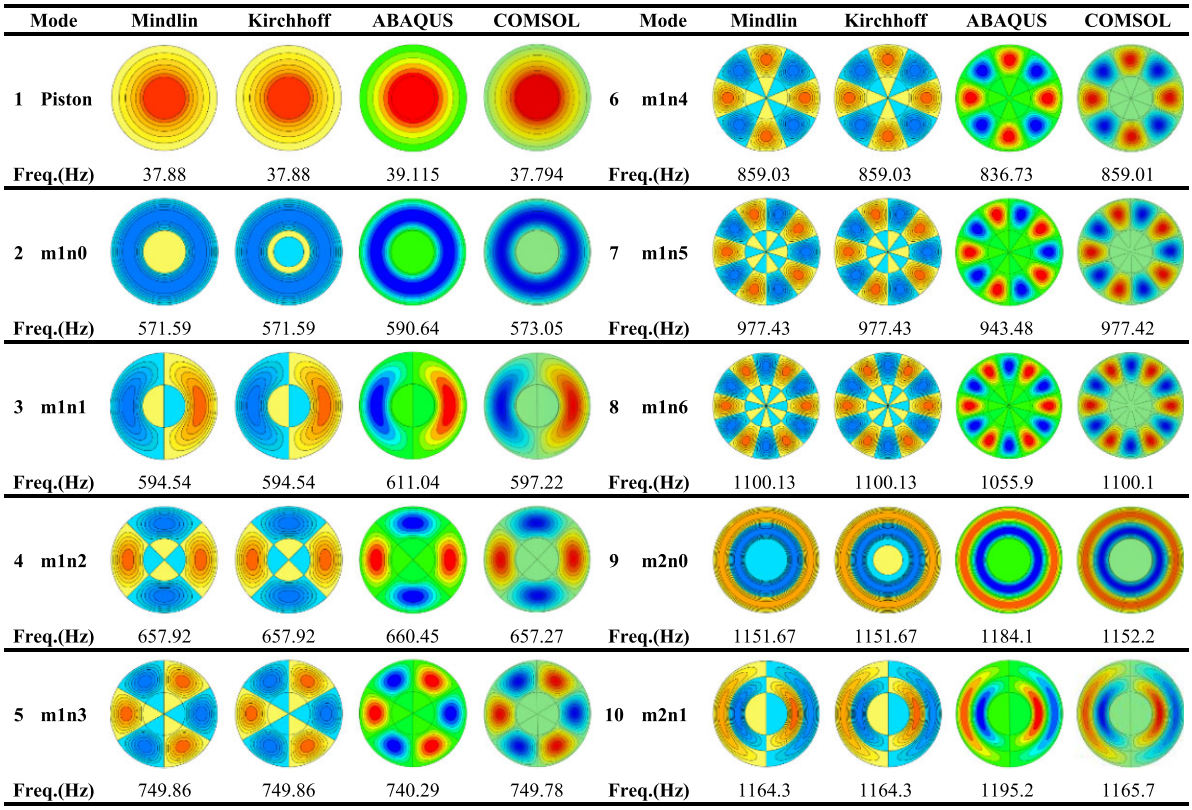

Figure 7 The first ten modes comparison result of type E structure obtained from theory and FEM.

Table 9 First 10 resonant frequencies of type E.

	Frequency (Hz)				
Mode	**Mindlin**	**ABAQUS**	**Diff (%)**	**COMSOL**	**Diff (%)**
1	37.88	39.115	−3.26	37.794	0.23
2	571.59	590.64	−3.33	573.05	−0.26
3	594.54	611.04	−2.78	597.22	−0.45
4	657.92	660.45	−0.38	657.27	0.1
5	749.86	740.29	1.28	749.78	0.01
6	859.03	836.73	2.60	859.01	0.002
7	977.43	943.48	3.47	977.42	0.001
8	1100.13	1055.9	4.02	1100.1	0.003
9	1151.67	1184.1	−2.82	1152.2	−0.05
10	1164.3	1195.2	−2.65	1165.7	−0.12
	Frequency (Hz)				
Mode	**Kirchhoff**	**ABAQUS**	**Diff (%)**	**COMSOL**	**Diff (%)**
1	37.88	39.115	−3.26	37.794	0.23
2	571.59	590.64	−3.33	573.05	−0.26
3	594.54	611.04	−2.78	597.22	−0.45
4	657.92	660.45	−0.38	657.27	0.1
5	749.86	740.29	1.28	749.78	0.01
6	859.03	836.73	2.60	859.01	0.002
7	977.43	943.48	3.47	977.42	0.001
8	1100.13	1055.9	4.02	1100.1	0.003
9	1151.67	1184.1	−2.82	1152.2	−0.05
10	1164.3	1195.2	−2.65	1165.7	−0.12

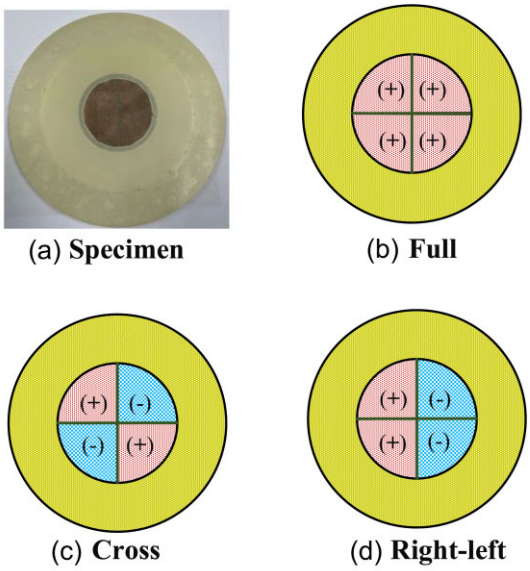

Figure 8 Schematic of designs of surface electrodes (a) Specimen, (b) Full, (c) Cross, (d) Right-Left (RL).

No.	Experiment	Mindlin	Kirchhoff	No.	Experiment	Mindlin	Kirchhoff
1				6			
Freq.(Hz)	10.3 (Full 0.3V)	10.29	10.29	Freq.(Hz)	988 (Full 10V)	989.77	990.22
2				7			
Freq.(Hz)	347 (Full 0.9V)	344.71	344.71	Freq.(Hz)	1085 (RL 5V)	1086.19	1089.07
3				8			
Freq.(Hz)	360 (RL 1.8V)	351.62	351.62	Freq.(Hz)	1931 (Cross 13V)	1930.85	1938.28
4				9			
Freq.(Hz)	376 (Cross 1.4V)	371.54	371.54	Freq.(Hz)	2157 (RL 7.6V)	2161.23	2163.9
5				10			
Freq.(Hz)	470 (Cross 1.4V)	459.42	460.07	Freq.(Hz)	2980 (Cross 20V)	2989.26	3004.39

Figure 9 The first ten modes obtained from AF-ESPI and compared with theoretical results for type A.

is the practical membrane part, and the area inside the red dotted line is part of the piezoceramic disk. Since the membrane and the piezoceramic disk must connect, the double-sided tape is chosen to bond those parts in the region between the red and blue dotted lines. The thickness of the double-sided tape is thin enough. Thus, the effect of the double-sided tape is ignored in the theoretical and numerical analysis.

In ABAQUS, the element type used for the membrane is M3D4R, and the mesh sizes are all 0.5 mm from the case of type A to type E. The element type used for the piezoceramic disk is C3D20RE. The mesh sizes for type A to type E are 0.5, 0.3, 0.5, 0.2 and 0.2 mm, respectively. A surface-based tie constraint is used to connect the membrane and disk; the tie region is given in Fig. 3. Then,

Table 10 First 10 experimental and theoretical resonant frequencies of type A.

No.	Frequency (Hz)				
	Experiment	Mindlin	Diff (%)	Kirchhoff	Diff (%)
1	10.3	10.29	0.1	10.29	0.1
2	347	344.71	0.66	344.71	0.66
3	360	351.62	2.38	351.62	2.38
4	376	371.54	1.2	371.54	1.2
5	470	459.42	2.25	460.07	2.11
6	988	989.77	−0.18	990.22	−0.22
7	1085	1086.19	−0.11	1089.07	−0.38
8	1931	1930.85	0.01	1938.28	−0.38
9	2157	2161.23	−0.2	2163.9	−0.32
10	2980	2989.26	−0.31	3004.39	−0.82

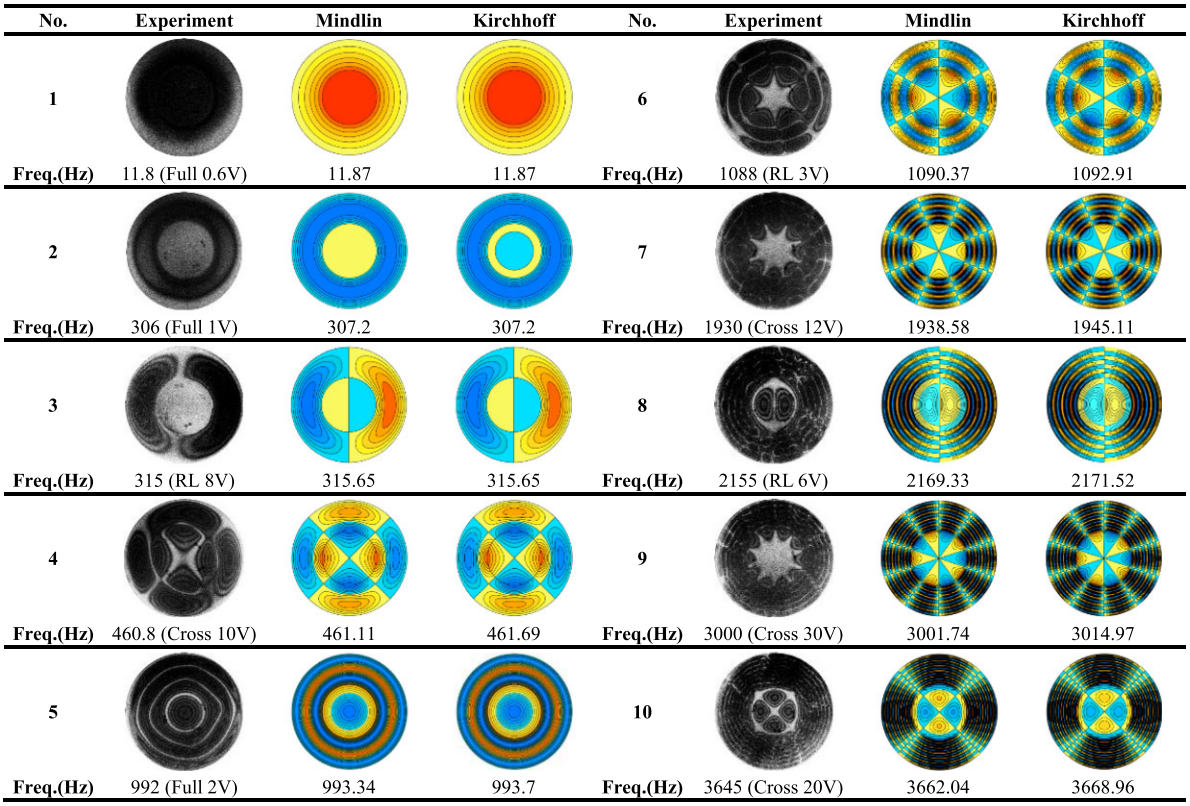

Figure 10 The first ten modes obtained from AF-ESPI and compared with theoretical results for type B.

two steps must be used in the analysis process: static and frequency in linear perturbation. In the static analysis step, the force was uniformly applied to the node points on the outer boundary of the annular membrane. The relation between the node force F_{node} and tension T can be given as

$$F_{node} = (2\pi bT)/N_{outer}, \tag{50}$$

where N_{outer} is the total node number on the outer boundary of the annular membrane. In the frequency analysis, the outer boundary of the annular membrane was set to be fixed. In COMSOL, the mesh sizes for the membrane part are all set as 0.5 mm for type A to E, and the mesh sizes for piezoceramic disks from type A to E are 0.3, 0.3, 0.3, 0.2, and 0.2 mm, respectively. In the annular membrane part, there needs to be an initial plane stress equal to the tension T, and the displacement field along the outer radius of the annular membrane must equal zero.

To measure the flexural mode shapes of the annular membrane internally connected with a piezoceramic disk, the AF-ESPI [20, 25] is used as Fig. 5 shows. A Helium-neon laser at a wavelength 632.8 nm is used as a coherent light source. The light goes through a spatial filter and then is split by a beam splitter into two parts. One illuminates the specimen; and the other illuminates the reference

Table 11 First 10 experimental and theoretical resonant frequencies of type B.

	Frequency (Hz)				
No.	**Experiment**	**Mindlin**	**Diff (%)**	**Kirchhoff**	**Diff (%)**
1	11.8	11.87	−0.59	11.87	−0.59
2	306	307.2	−0.39	307.2	−0.39
3	315	315.65	−0.21	315.65	−0.21
4	460.8	461.11	−0.07	461.69	−0.19
5	992	993.34	−0.14	993.7	−0.17
6	1088	1090.37	−0.22	1092.91	−0.45
7	1930	1938.58	−0.44	1945.11	−0.78
8	2155	2169.33	−0.66	2171.52	−0.77
9	3000	3001.74	−0.06	3014.97	−0.5
10	3645	3662.04	−0.47	3668.96	−0.66

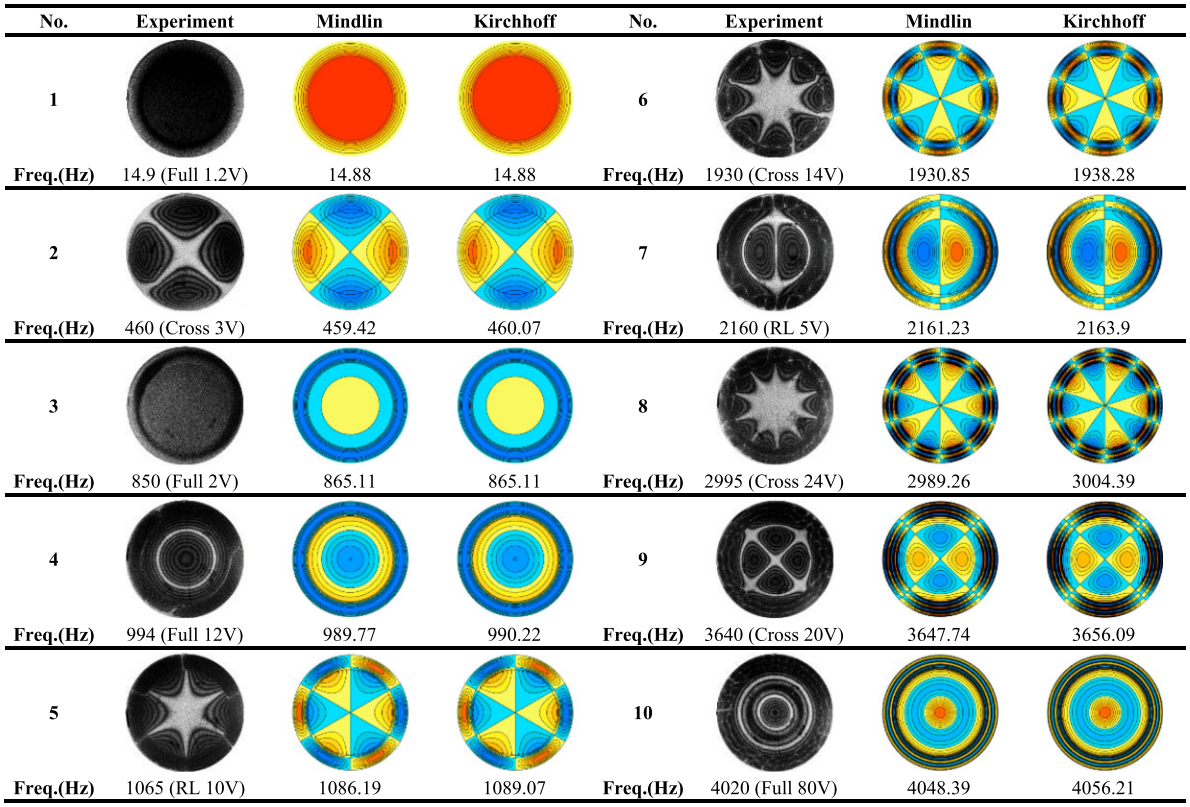

Figure 11 The first ten modes obtained from AF-ESPI and compared with theoretical results for type C.

plate. The deformation of the specimen leads to phase changes in the light field of the specimen. The phase changes result in the interference fringes with bright and dark distributions. A function generator is connected with a power amplifier, and then connected with surface electrodes on the piezoceramic disk.

3.2. Theoretical, numerical and experimental results

There are two types of modes: the piston mode and the coupled mode. The piston mode is that the piezoceramic disk is equivalent to a block of mass, so the structure vibration behavior of the piston can be equal to an annular membrane with a clamped boundary along the outside radius and internally connected with a mass block. The coupled mode means the displacement fields of the membrane part and piezoceramic disk interact. Due to the significant difference in stiffness between the membrane and the piezoelectric material, the coupled mode can be further classified into two vibration forms: one is dominated by the annular membrane, and the dynamic behavior of the piezoceramic disk characterizes the other. The vibration modes dominated by the membrane (membrane-dominated mode) exhibit significantly more minor deformation in the piezoceramic disk compared to the membrane part. Therefore, this vibration behavior approximates an annular membrane with both inner and outer radii fixed. On the contrary, the piezoceramic-dominated modes referred to the deformation of the piezoceramic disk, which is relatively more significant in the composite structures. At this

Table 12 First 10 experimental and theoretical resonant frequencies of type C.

	Frequency (Hz)				
No.	**Experiment**	**Mindlin**	**Diff (%)**	**Kirchhoff**	**Diff (%)**
1	14.9	14.88	0.13	14.88	0.13
2	460	459.42	0.13	460.07	−0.02
3	850	865.11	−1.78	865.11	−1.78
4	994	989.77	0.43	990.22	0.38
5	1065	1086.19	−1.99	1089.07	−2.26
6	1930	1930.85	−0.04	1938.28	−0.43
7	2160	2161.23	−0.06	2163.9	−0.18
8	2995	2989.26	0.19	3004.39	−0.31
9	3640	3647.74	−0.21	3656.09	−0.44
10	4020	4048.39	−0.71	4056.21	−0.9

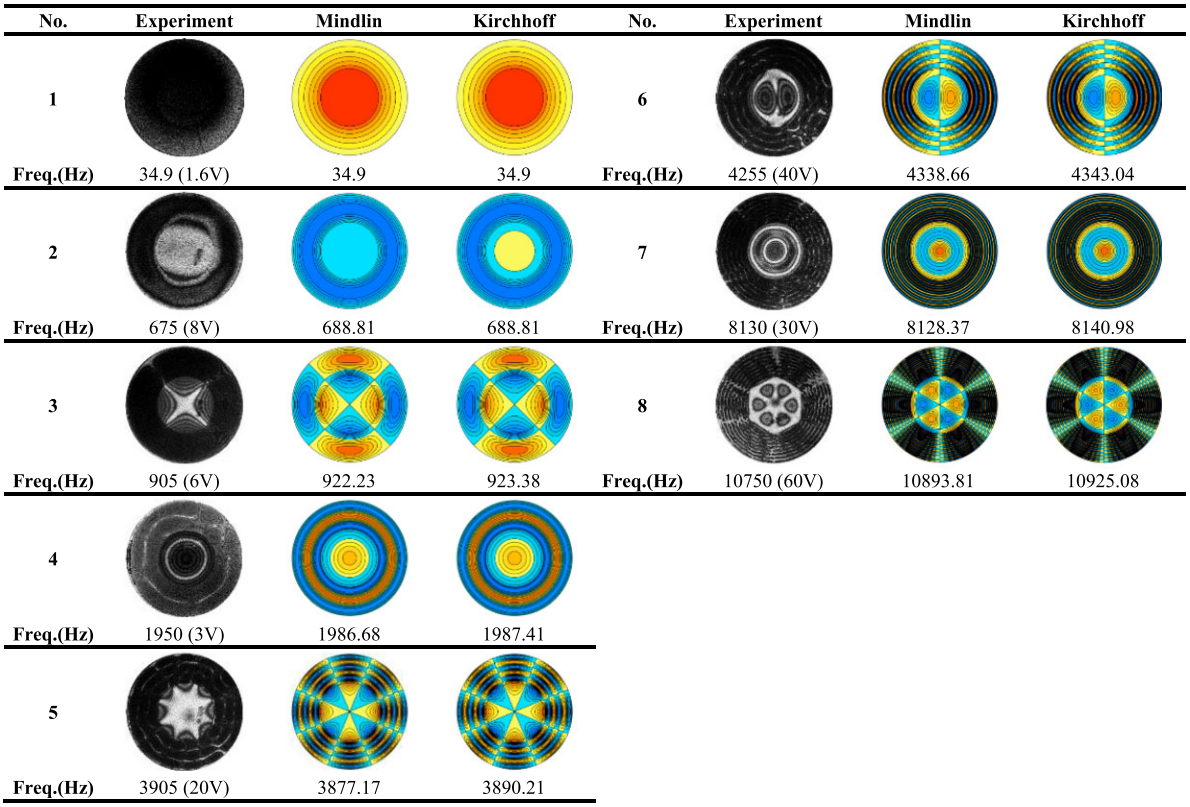

Figure 12 The first eight modes obtained from AF-ESPI and compared with theoretical results for type D.

point, the resonant frequencies of the structure for piezoceramic-dominated modes closely align with the natural frequencies of a piezoceramic disk with an entirely free boundary condition.

The first 10 theoretical and numerical resonant frequencies and mode shapes of type A are shown in Fig. 6. In the mode shapes, the red region means the positive displacement, and the blue region means the negative displacement. In the figures, "Mindlin" means that the result is obtained from Mindlin plate theory for ceramic disks. "Kirchhoff" represents the result obtained from Kirchhoff's plate assumption for ceramic disks. "ABAQUS" and "COMSOL" indicate the results are obtained from the software ABAQUS and COMSOL, respectively. "Piston" means the mode is piston mode. Mode 1 is the piston mode. The other modes are coupled mode. The character "m" means the number of nodal circles, and the character "n" means the number of nodal lines. For example, "m2n2" for mode 7 in Fig. 6 means the mode has two nodal circles and two nodal lines. For mode 2, "Kirchhoff" predicts one more nodal circle than other methods. This result is because the displacement near the disk's center is minimal; thus, the numerical error will induce one more nodal circle in this case. According to the displacement distribution of mode shapes, mode 7 is the piezoceramic-dominated mode, and the rest of the modes are denoted as the membrane-dominated modes.

Table 4 shows the first 10 resonant frequencies of type A. Table 5 shows the first ten resonant frequencies of a completely free piezoceramic disk with the same sizes as type A and a clamped-clamped annular membrane with the same sizes as type A. It can be

Table 13 First eight experimental and theoretical resonant frequencies of type D.

	Frequency (Hz)				
No.	**Experiment**	**Mindlin**	**Diff (%)**	**Kirchhoff**	**Diff (%)**
1	34.9	34.9	0	34.9	0
2	675	688.81	−2.05	688.81	−2.05
3	905	922.23	−1.9	923.38	−2.03
4	1950	1986.68	−1.88	1987.41	−1.92
5	3905	3877.17	0.71	3890.21	0.38
6	4255	4338.66	−1.97	4343.04	−2.07
7	8130	8128.37	0.02	8140.98	−0.14
8	10 750	10 893.81	−1.34	10925.08	−1.63

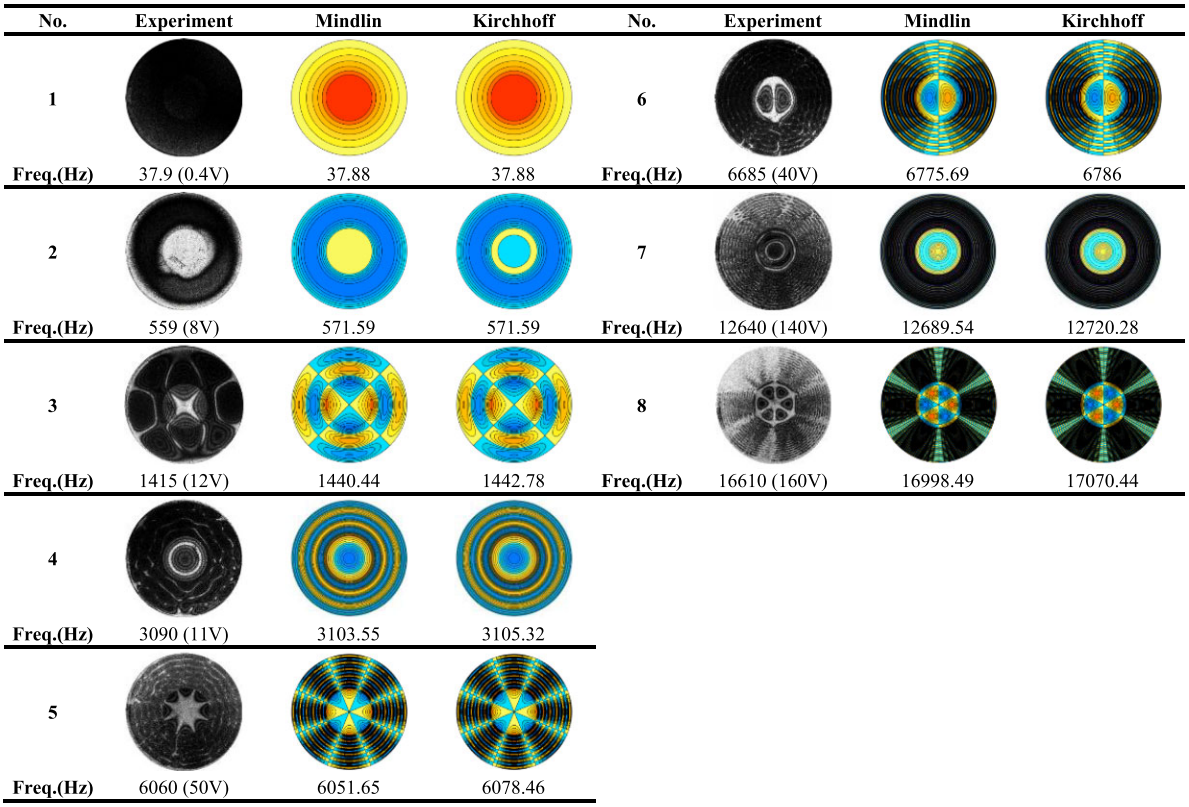

Figure 13 The first eight modes obtained from AF-ESPI and compared with theoretical results for type E.

found that the resonant frequencies of piezoceramic-dominated mode is very close to the natural frequencies of the piezoceramic disk with the free boundary condition. The resonant frequencies of membrane-dominated modes are close to the natural frequencies of the clamped-clamped annular membrane. In Table 4, "Kirchhoff" and "Mindlin" predict larger difference for resonant frequencies compared with "ABAQUS" than those compared with "COMSOL". Mode 10 has the largest difference between "ABAQUS" and the two theories. The largest difference is 8.65%. Mode 7 has the smallest difference. The difference between "ABAQUS" and "Mindlin" is −0.23%. And the difference between "ABAQUS" and "Kirchhoff" is −0.1%. Mode 4 has the largest difference between "COMSOL" and the two theories. The largest difference is 0.24%. Mode 9 has the smallest difference. It is about 0%.

Table 6 shows the first 10 resonant frequencies of type B. The mass of the piezoceramic disk decreases when compared with type A, the resonant frequency of the piston mode increases. Mode 10 has the largest difference between "ABAQUS" and the two theories. The largest difference is 7.93%. Mode 7 has the smallest difference. The difference between "ABAQUS" and "Mindlin" is 0.13%. And the difference between "ABAQUS" and "Kirchhoff" is 0.26%. Mode 4 has the largest difference between "COMSOL" and the two theories. The largest difference is 0.21%. Mode 9 has the smallest difference. It is about 0%. Table 7 shows the first ten resonant frequencies of type C. The outer radius of the annular membrane decreases when compared with type A, the resonant frequency of the piston mode increases. Mode 10 has the largest difference between "ABAQUS" and the two theories. The largest difference is 3.39%. Mode 2 has the smallest difference. The difference between "ABAQUS" and "Mindlin" is −0.06%. And the difference between "ABAQUS" and "Kirchhoff" is 0.08%. Mode 6 has the largest difference between "COMSOL" and the two theories. The largest difference is 0.16%.

Table 14 First eight experimental and theoretical resonant frequencies of type E.

	Frequency (Hz)				
No.	**Experiment**	**Mindlin**	**Diff (%)**	**Kirchhoff**	**Diff (%)**
1	37.9	37.88	0.05	37.88	0.05
2	559	571.59	−2.25	571.59	−2.25
3	1415	1440.44	−1.8	1442.78	−1.96
4	3090	3103.55	−0.44	3105.32	−0.5
5	6060	6051.65	0.14	6078.46	−0.3
6	6685	6775.69	−1.36	6786	−1.51
7	12 640	12 689.54	−0.39	12720.28	−0.64
8	16 610	16 998.49	−2.34	17070.44	−2.8

Mode 10 has the smallest difference 0.002%. Mode 1 is the piston mode. Mode 7 is the piezoceramic-dominated mode. The others are membrane-dominated modes.

Table 8 shows the first ten resonant frequencies of type D. Mode 10 has the largest difference between "ABAQUS" and the two theories. The largest difference is 6.47%. The smallest difference occurs at mode 4, the difference is −0.4%. Mode 4 has the largest difference between "COMSOL" and the two theories 0.63%. Mode 10 has the smallest difference −0.002%. The first 10 theoretical and numerical resonant frequencies and mode shapes of type E are shown in Fig. 7. Table 9 shows the first 10 resonant frequencies of type E. Mode 8 has the largest difference between "ABAQUS" and the two theories. The largest difference is 4.02%. Mode 4 has the smallest difference −0.38%. Mode 3 has the largest difference between "COMSOL" and the two theories −0.45%. Mode 7 has the smallest difference 0.001%. Generally, "COMSOL" predicts more accurate resonant frequencies than "ABAQUS" compared with theories. It is recommended to use "COMSOL" to simulate the coupled model for membrane and piezoelectric plates.

In the experiments, the two opposite faces of the piezoceramic disk are covered with thin silver electrodes. Three types of surface electrodes named "Full," "Cross," and "Right-Left (RL)" are shown in Fig. 8. The same symbols "+" or "−" mean that the electric voltages are in the same phase. The different symbols mean that the electric voltages are out-of-phase. The first 10 theoretical and experimental resonant frequencies and mode shapes of type A are shown in Fig. 9. The type of surface electrodes and the excitation electric voltage are shown in the figure. The high frequency mode shapes of the membrane are difficult to excite. Mode 1 is the piston mode, modes 2–4 are membrane-dominated modes, and the others are piezoceramic-dominated modes. The experimental and theoretical resonant frequencies for type A are listed in Table 10. The maximum difference between theories and experiment is 2.38% for mode 3. The minimum difference between "Kirchhoff" and the experiment is 0.1% for the piston mode. And the minimum difference between "Mindlin" and experiment is 0.01% for mode 8. The first ten theoretical and experimental resonant frequencies and mode shapes of type B are shown in Fig. 10. The experimental and theoretical resonant frequencies for type B are listed in Table 11. The maximum and minimum differences between "Kirchhoff" and experiment are −0.78% for mode 7 and −0.17% for mode 5, respectively. The maximum and minimum differences between "Mindlin" and experiment are −0.66% for mode 8 and −0.06% for mode 9, respectively. The first 10 theoretical and experimental resonant frequencies and mode shapes of type C are shown in Fig. 11. The experimental and theoretical resonant frequencies for type C are listed in Table 12. Mode 1 is the piston mode. Mode 3 is the membrane-dominated modes. The others represent the piezoceramic-dominated modes. The maximum and minimum differences between "Kirchhoff" and experiment are −2.26% for mode 5 and −0.02% for mode 2, respectively. The maximum and minimum differences between "Mindlin" and experiment are −1.99% for mode 5 and −0.04% for mode 6, respectively. The first eight theoretical and experimental resonant frequencies and mode shapes of type D are shown in Fig. 12. The experimental and theoretical resonant frequencies for type D are listed in Table 13. Since the piezoceramic disk is too thin, it is difficult to split electrodes, and the excitation method "Full" can only be used for type D. According to the experimental results, the piston motion occurs at the first mode. Mode 2 is the membrane-dominated modes, and the others are piezoceramic-dominated modes. The maximum and minimum differences between "Kirchhoff" and experiment are −2.07% for mode 6 and 0% for the piston mode, respectively. The maximum and minimum differences between "Mindlin" and experiment are −2.05% for mode 2 and 0% for the piston mode, respectively. The first eight theoretical and experimental resonant frequencies and associated mode shapes of type E are given in Fig. 13. The experimental and theoretical resonant frequencies for type E are listed in Table 14. The maximum and minimum differences between "Kirchhoff" and experiment are −2.8% for mode 8 and 0.05% for the piston mode, respectively. The maximum and minimum differences between "Mindlin" and experiment are −2.34% for mode 8 and 0.05% for the piston mode, respectively.

4. CONCLUSION

This study proposed a novel and comprehensive analytical solution for an annular membrane internally connected with a piezoceramic disk structure. The vibration characteristics of the composite structures are analyzed, and the accuracy of the theoretical analysis, numerical calculation and experimental measurement is also verified. First, the general solution for the free vibration of an annular membrane under uniform tension was derived. Next, the theoretical solutions based on Kirchhoff and Mindlin plate theories for the

piston modes and coupled modes of an annular membrane internally connected with a piezoceramic disk were derived. According to the significant difference in stiffness between the membrane and the piezoelectric material, the coupled modes can be further classified into membrane-dominated and piezoceramic-dominated modes. Then, the theoretical results are compared with the numerical results obtained from two finite element software packages: ABAQUS and COMSOL. After that, the AF-ESPI was used to measure the mode shapes of five specimens with different sizes.

Based on the comparison between theoretical, numerical and experimental methods, it is found that the resonant frequencies and associated mode shapes of membrane-dominated modes are approximate to an annular membrane with both inner and outer radii fixed, and the difference between theoretical and experimental results are unrelated to the Kirchhoff and Mindlin plate theories. In contrast, the piezoceramic-dominated modes can significantly differ in the prediction of resonant frequencies due to the different assumptions of the two plate theories. It is found that the results obtained from COMSOL are consistent with the prediction of theoretical analysis in both membrane-dominated modes and piezoceramic-dominated modes. Compared to experimental and theoretical results, the minor discrepancies of resonant frequencies obtained from ABAQUS only occur in predicting the piezoceramic-dominated modes. Since the comparison of theoretical, numerical and experimental results was in good agreement, the validity of the proposed analytical solution in this study can be verified. In addition, the proposed theoretical method can be applied to the optimal design of speakers, micro pumps, and biomedical technologies.

ACKNOWLEDGEMENTS

The authors appreciate the financial support provided to this study by the Ministry of Science and Technology (Republic of China) under Grant No. MOST 111-2221-E-194-027-MY2 and MOST-110-2223-E-002-005-MY3. The study was also partially supported by the Advanced Institute of Manufacturing with High-Tech Innovations (AIM-HI) under The Featured Areas Research Center Program within the framework of the Higher Education Sprout Project of the Ministry of Education (MOE) in Taiwan.

CONFLICT OF INTEREST

None declared.

REFERENCES

1. Chiang HY, Huang YH. Resonance mode and sound pressure produced by circular diaphragms of electrostatic and piezoelectric speakers. *Applied Acoustics* 2018;**129**:365–378.
2. Ashraf MW, Tayyaba S, Afzulpurkar N. Micro electromechanical systems (MEMS) based microfluidic devices for biomedical applications. *International Journal of Molecular Sciences* 2011;**12**(6):3648–3704.
3. Bußmann AB, Durasiewicz CP, Kibler SHA, Wald CK. Piezoelectric titanium based microfluidic pump and valves for implantable medical applications. *Sensors and Actuators A: Physical* 2021;**323**:112649.
4. Calderon M, Reyes-Betanzo C. Design and simulation of a piezoelectric micropump for drug delivery systems. *Microsystem Technologies* 2023;**29**(2):253–264.
5. Jenkins CHM, Korde UA. Membrane vibration experiments: an historical review and recent results. *Journal of Sound and Vibration* 2006;**295**(3–5):602–613.
6. Rayleigh JWSB. *The Theory of Sound*. New York, USA: Macmillan, 1896.
7. Mei C. Free Vibrations of circular membranes under arbitrary tension by the finite-element method. *The Journal of the Acoustical Society of America* 1969;**46**(3B):693–700.
8. Nagaya K, Hai Y. Free vibration of composite membranes with arbitrary shape. *Journal of Sound and Vibration* 1985;**100**(1):123–134.
9. Jabareen M, Eisenberger M. Free vibrations of non-homogeneous circular and annular membranes. *Journal of Sound and Vibration* 2001;**240**(3):409–429.
10. Bahrami A, Ilkhani MR, Bahrami MN. Wave propagation technique for free vibration analysis of annular circular and sectorial membranes. *Journal of Vibration and Control* 2015;**21**(9):1866–1872.
11. Bahrami A, Teimourian A. Free vibration analysis of composite, circular annular membranes using wave propagation approach. *Applied Mathematical Modelling* 2015;**39**(16):4781–4796.
12. Liu X, Zhao X, Xie C. Exact free vibration analysis for membrane assemblies with general classical boundary conditions. *Journal of Sound and Vibration* 2020;**485**:115484.
13. Mindlin RD. Forced thickness-shear and flexural vibrations of piezoelectric crystal plates. *Journal of Applied Physics* 1952;**23**(1):83–88.
14. Lee PCY, Syngellakis S, Hou JP. A two-dimensional theory for high-frequency vibrations of piezoelectric crystal plates with or without electrodes. *Journal of Applied Physics* 1987;**61**(4):1249–1262.
15. Ding HJ, Xu RQ, Chi YW, Chen WQ. Free axisymmetric vibration of transversely isotropic piezoelectric circular plates. *International Journal of Solids and Structures* 1999;**36**(30):4629–4652.
16. Heyliger PR, Ramirez G. Free vibration of laminated circular piezoelectric plates and discs. *Journal of Sound and Vibration* 2000;**229**(4):935–956.
17. Duan WH, Quek ST, Wang Q. Free vibration analysis of piezoelectric coupled thin and thick annular plate. *Journal of Sound and Vibration* 2005;**281**(1–2):119–139.
18. Hosseini-Hashemi S, Es'Haghi M, Taher HRD. An exact analytical solution for freely vibrating piezoelectric coupled circular/annular thick plates using Reddy plate theory. *Composite Structures* 2010;**92**(6):1333–1351.

19. Huang YH, Ma CC, Li ZZ. Investigations on vibration characteristics of two-layered piezoceramic disks. *International Journal of Solids and Structures* 2014;**51**(1):227–251.
20. Wu YC, Huang YH, Ma CC. Theoretical analysis and experimental measurement of flexural vibration and dynamic characteristics for piezoelectric rectangular plate. *Sensors and Actuators A: Physical* 2017;**264**:308–332.
21. Huang CH, Li CC, Wu YC, Ma CC. Theoretical analysis of transverse and planar vibrations for the piezoceramic disk based on Mindlin plate theory. *Applied Mathematical Modelling* 2021;**97**:568–587.
22. Ji M, Wu YC, Ma CC. In-plane-dominated vibration characteristics of piezoelectric thick circular plates based on higher-order plate theories. *Journal of Mechanics* 2022;**38**:410–432.
23. Wu YC. Accurate dynamic electromechanical solution for rectangular piezoelectric plate based on modified FSDT. *International Journal of Structural Stability and Dynamics* 2023:2350181. https://doi.org/10.1142/S021945542350181X
24. Lien IC, Lo YC, Chiu SH, Shu YC. Comparison between overall and respective electrical rectifications in array of piezoelectric energy harvesting. *Journal of Mechanics* 2022;**38**:518–530.
25. Ma CC, Huang CH. The investigation of three-dimensional vibration for piezoelectric rectangular parallelepipeds using the AF-ESPI method. *IEEE Transactions on Ultrasonics, Ferroelectrics, and Frequency Control* 2001;**48**(1):142–153.
26. Huang CH, Lin YC, Ma CC. Theoretical analysis and experimental measurement for resonant vibration of piezoceramic circular plates. *IEEE Transactions on Ultrasonics, Ferroelectrics, and Frequency Control* 2004;**51**(1):12–24.
27. Huang CH, Ma CC, Lin YC. Theoretical, numerical, and experimental investigation on resonant vibrations of piezoceramic annular disks. *IEEE Transactions on Ultrasonics, Ferroelectrics, and Frequency Control* 2005;**52**(8):1204–1216.
28. Ma CC, Lin HY, Lin YC, Huang YH. Experimental and numerical investigations on resonant characteristics of a single-layer piezoceramic plate and a cross-ply piezolaminated composite plate. *The Journal of the Acoustical Society of America* 2006;**119**(3):1476–1486.
29. Krushynska A, Meleshko V, Ma CC, Huang YH. Mode excitation efficiency for contour vibrations of piezoelectric resonators. *IEEE Transactions on Ultrasonics, Ferroelectrics, and Frequency Control* 2011;**58**(10):2222–2238.
30. Wang CY. Vibration of an annular membrane attached to a free, rigid core. *Journal of Sound and Vibration* 2003;**260**(4):776–782.
31. Pinto F. Analytical and experimental investigation on a vibrating annular membrane attached to a central free, rigid core. *Journal of Sound and Vibration* 2006;**291**(3–5):1278–1287.
32. Langfeldt F, Gleine W, von Estorff O. Analytical model for low-frequency transmission loss calculation of membranes loaded with arbitrarily shaped masses. *Journal of Sound and Vibration* 2015;**349**:315–329.
33. Weaver W, Jr, Timoshenko SP, Young DH. *Vibration Problems in Engineering*. New York, USA: John Wiley & Sons, 1991.
34. Ji M, Wu YC, Ma CC. Theoretical analyses and numerical simulation of flexural vibration based on Reddy and modified higher-order plate theories for a transversely isotropic circular plate. *Acta Mechanica* 2021;**232**(7):2825–2842.
35. Ji M, Wu YC, Ma CC. Analytical solutions for in-plane dominated vibrations of transversely isotropic circular plates based on high-order theories. *Journal of Sound and Vibration* 2021;**503**:116110.

Received: 5 November 2023; **Accepted:** 1 December 2023